Published in final edited form as:
Biochemistry. 2006 November 28; 45(47): 14192–14200. doi:10.1021/bi060802s.

Uncoupling of nucleotide flipping and DNA bending by the T4-pyrimidine dimer DNA glycosylase[+]

Randall K. Walker[‡], **Amanda K. McCullough**[§], and **R. Stephen Lloyd**[§]

‡ *Perkin Elmer Life and Analytical Sciences, Boston MA*

§ *Center for Research on Occupational and Environmental Toxicology and Department of Molecular & Medical Genetics, Oregon Health & Science University, Portland OR 97239-3098*

Abstract

Bacteriophage T4 pyrimidine dimer glycosylase (T4-Pdg) is a base excision repair protein that incises DNA at cyclobutane pyrimidine dimers that are formed as a consequence of exposure to ultraviolet light. Cocrystallization of T4-Pdg with substrate DNA has shown that the adenosine opposite the 5′ thymine of a thymine-thymine (TT) dimer is flipped into an extrahelical conformation and that the DNA backbone is kinked 60° in the enzyme-substrate (ES) complex. To examine the kinetic details of the pre-catalytic events in the T4-Pdg reaction mechanism, investigations were designed to separately measure nucleotide flipping and DNA bending. The fluorescent adenine base analog, 2-aminopurine (2-AP) placed opposite an abasic site analog, tetrahydrofuran, exhibited a 2.8 fold increase in emission intensity when flipped in the ES complex. Using the 2-AP fluorescence signal for nucleotide flipping, k_{on} and k_{off} presteady-state kinetic measurements were determined. DNA bending was measured by fluorescence resonance energy transfer using fluorescent donor/acceptor pairs located at the 5′ ends of oligonucleotides in duplex DNA. The fluorescence intensity of the donor fluorophore was quenched by 15% in the ES complex as a result of an increased efficiency of energy transfer between the labeled ends of the DNA in the bent conformation. Kinetic analyses of the bending signal revealed an off rate that was 2.5 fold faster than the off rate for nucleotide flipping. These results demonstrate that the nucleotide flipping step can be uncoupled from the bending of DNA in the formation of an ES complex.

In most organisms, the primary mechanism for the repair of ultraviolet light (UV[1])-induced DNA photoproducts is the nucleotide excision repair pathway (NER) (1). However, in a modest subset of bacteria, and in some bacteriophage and viruses that infect eukaryotic cells, repair of the major UV photoproducts, the *cis-syn* cyclobutane pyrimidine dimers (CPD) can be initiated through the base excision repair (BER) pathway (reviewed in (2)). The initiation of BER at this dipyrimidine lesion is catalyzed by pyrimidine dimer glycosylases (Pdgs) (3). The most extensively characterized of these enzymes is the bacteriophage T4-Pdg. Pre- and post-catalytic events as measured by X-ray crystallography and fluorescence spectroscopy include flipping of the purine opposite the 5′ pyrimidine of the dimer into a cleft on the surface of the enzyme and bending of the DNA to a 60° angle (4,5). Once bound to a dimer site, T4-Pdg utilizes the α-NH_2 group of Thr2 and Glu23 to cleave the glycosyl bond of the 5′ dimer pyrimidine and the phosphodiester backbone *via* β-elimination reaction (6–10).

[+]This research was supported by National Institutes of Health Grant ES04091 and P30 ES06676.

*To whom correspondence should be addressed. Phone: (503) 494-9957. Fax: (503) 494-6831. Email: E-mail: lloydst@ohsu.edu.

[1]**Abbreviations:** BER, base excision repair; CPD, cyclobutane pyrimidine dimer; ES, enzyme-substrate; NER, nucleotide excision repair; pdg, OGG1, 8-oxoguanine DNA glycosylase; pyrimidine dimer glycosylase; T4-pdg, bacteriophage T4 pyrimidine dimer glycosylase; UDG; uracil DNA glycosylase; UV, ultraviolet; 2-AP, 2-aminopurine.

The co-crystal structure of T4-Pdg with CPD-containing DNA was the first evidence of nucleotide flipping by a DNA repair enzyme (5) and recently, we have solved the cocrystal structure of T4-pdg complexed as a reduced-imine intermediate with abasic site-containing DNA (11). In the intervening time, the co-crystal structures of flipped and covalently bound complexes have been solved for several other DNA glycosylases including uracil DNA glycosylases UDGs (12,13), 3-methyladenine DNA glycosylase (14), 3-methyladenine DNA glycosylase (AlkA) (15), 8-oxoguanine DNA glycosylase (OGG1) (16,17), formamidopyrimidine DNA glycosylase (FPG) (18–20), and endonuclease VIII (21,22). A common property of these co-crystal complexes is that specific amino acids occupy the “hole” in DNA that had been previously occupied by the extrahelical base. In the cases of T4-Pdg complexes, it was shown that the side chains of Arg22 and Arg26 partially fill the space previously occupied by the flipped nucleotide (5,11). In the covalently bound structure, the side chains of Arg22 and Arg26 were further embedded in the intrahelical volume created by nucleotide flipping in the enzyme-DNA complex. Conceptually similar proposals have been made for 1) *M. HhaI* using Gln237 as part of a push and bind mechanism (23); 2) *E. coli* and human UDG using a Ser-Pro pinch and leucine residue as a hydrophobic wedge mechanism (24–27), and 3) *E. coli* MutY DNA glycosylase using Gly116, Gly118 and Gly79, Gly81 in a bend and pinch mechanism (28).

The biochemical and mechanistic studies of the catalytic mechanism of T4-Pdg have served as the paradigm for other glycosylase enzymes despite its unique feature of flipping the nucleotide opposite the lesion, rather than the damaged base itself. Our prior investigations on the precatalytic events in the T4-Pdg reaction utilized both non-cleavable, high affinity DNA substrates and catalytically inactive T4-Pdg mutants. Verdine and his colleagues have synthesized the former by designing transition state analogues for DNA glycosylases (29,30). Using one of these substrates, a pyrrolidine-containing DNA and other synthetic AP sites (tetrahydrofuran or reduced AP site), we established that T4-Pdg binds with high affinity to these DNAs (31). These data provided the rationale for a fluorescence assay to monitor nucleotide flipping. This was achieved by positioning a 2-AP opposite either the synthetic AP site or CPD (4). Nucleotide flipping of the 2-AP resulted in a fluorescence enhancement as it moved from a quenched, stacked position within the DNA to the solvent exposed surface of the protein. In addition, in contrast to what had been previously hypothesized, investigation of mutant T4-Pdg proteins demonstrated that specific binding does not require nucleotide flipping for complex stabilization, i.e. specific binding could be uncoupled from nucleotide flipping (4).

The exquisite selectivity of this assay was demonstrated by moving the 2-AP opposite the (nonscissile) 3′-base of the CPD in which no fluorescence enhancements were observed. These results suggest that in the case of the T4-pdg there is little general helical distortion that would give rise to the enhanced 2-AP fluorescence and thus, its use as a measure of base flipping is well justified. However, it should be noted that in some cases, the 2-AP-based fluorescent assay is not a clear indicator of base flipping in that, while some methyltransferases cause a significant enhancement in 2-AP fluorescence upon binding to a target site, others do not (32,33). Likewise, DNA distortions from events other than base flipping may lead to an enhanced 2-AP fluorescence (34).

The fluorescent properties of 2-AP have been used in analyzing the reaction mechanisms of a variety of other DNA reactive enzymes, including, but not limited to, UDG (35–37), photolyase (38–40), and as indicated above, several methyltransferases (32,41–43). Collectively, these studies have revealed that these enzymes use a variety of mechanisms to achieve DNA bending and extrahelical movement of a nucleotide, ranging from a near simultaneous expulsion of the base and DNA bending, to temporally uncoupled precatalytic events. Since T4-Pdg is the only enzyme demonstrated to flip the nucleotide opposite the catalytic site and is known to severely

kink DNA at the damaged site, we have developed an experimental strategy that allows analyses of nucleotide flipping and substrate duplex DNA bending by this protein. This design builds off our previous strategy using 2-AP as a fluorescent reporter combined with fluorescent resonance energy transfer. The current investigation reveals a temporal uncoupling of the T4-Pdg-induced DNA bending and nucleotide flipping.

EXPERIMENTAL PROCEDURES

Materials

TAMRA-5-SE and QSY-7-SE were purchased from Molecular Probes (Eugene, OR). 5′-Amino modifier 5, dSpacer tetrahydrofuran and 2-aminopurine CE phosphoramidites were purchased from Glen Research (Sterling VA). 3-[(3-Cholamidopropyl) dimethylammonio]-1-propanesulfonate (CHAPS) was obtained from Boehringer Mannheim. Heparin grade I-A (porcine mucosa) was purchased from Sigma (St. Louis, MO).

Enzyme Expression and Purification

T4-Pdg was cloned, expressed and purified as previously described (44). The purified enzyme was stored at 4° C in 25 mM $NaHPO_4$ (pH 7.0), 25 mM NaCl, and 1 mM EDTA. Protein concentrations were determined from absorbance readings at 280 nm (minus 1.7 times the A320 reading to correct for any scatter), using a calculated molar extinction coefficient of 15,930 (45).

Oligonucleotide synthesis

All oligonucleotides were synthesized in the Molecular Genetics Core facility (University of Texas Medical Branch, Galveston, TX) on a Perseptive Biosystems Expedite model 8909 instrument using 1 μmole 1000 A CPG columns. Crude synthates were purified by SPE on a Waters SepPak followed by RP (C18) HPLC with product identity confirmed by MALDI/MS. Purified oligonucleotides were lyophilized and stored at −20° C.

Oligonucleotide labeling

Purified lyophilized 5′-amino modified oligonucleotides were resuspended in 10 mM Tris HCl (pH 8.0), 100 mM NaCl, 0.1 mM EDTA (TEN buffer) and concentrations were determined by A260 measurements (1 OD=50 μg/ml). A volume containing 100 μg of oligonucleotide was twice precipitated by the addition of 2.5 volumes ethanol with 10 mM $MgCl_2$, centrifuged and resupended in 85 μl of 0.2 M sodium borate (pH 8.5). The succinimidyl ester reactive dyes were dissolved in anhydrous acetonitrile, split into microfuge tubes in 250 μg aliquots, dried under vacuum in a SpeedVac and stored at −20° C. Oligonucleotide labeling was performed by redissolving 250 μg of the reactive dye in 15 μl DMSO and mixing with 100 μg oligonucleotide in 85 μl borate buffer. Reactions proceeded ~18 h at 22° C, adjusted to 0.3 M NaCl, 10 mM $MgCl_2$, twice precipitated with ethanol, and the DNA resuspended in a final volume of 100 μl TEN. The labeled DNAs were further purified through BioSpin 6 columns (BioRad) that were previously equilibrated in TEN. Final purification was carried out by RP HPLC (250 × 4.6 mm Phenomenex Jupiter 300 A C4) using a linear gradient of 0.1M triethylamine acetate, (pH 7.0) to 60% acetonitrile developed over 60 min at 1 ml/min. The labeled oligonucleotide was collected, lyophilized and stored at −20° C.

Oligonucleotide Annealing

HPLC purified oligonucleotides were resuspended in TEN and concentrations were estimated by A260 measurements. A typical annealing reaction consisted of the TAMRA-labeled oligonucleotide strand mixed with a 1.1 fold molar excess of the unlabeled strand or QSY labeled strand, heated to 90° C and allowed to slow cool to 4° C using a PCR instrument.

Duplex oligonucleotides were isolated from single-stranded DNA by anion exchange HPLC (250×4.6 mm SynchroPak AX 300), using a linear gradient of 10 mM potassium phosphate (pH 7.0), 0.1 mM EDTA (Buffer A) to 2 M KCl in buffer A in 60 min at 1 ml/min. The duplex containing peak was collected and concentrated in a Centricon YM-3 filter (Amicon) and exchanged into TEN buffer using the same centrifugation filtration device.

Fluorescence Measurements

All fluorescence measurements were performed on a SPEX Fluorolog-2 spectrofluorometer (Edison, NJ) with data acquisition in the photon counting mode and with sample temperatures maintained at 25° C by a circulating water bath.

Emission Spectra

Ratiometric spectra were collected at 1 nm intervals with 1 s integration per step. Sample spectra were collected in 220 μl in PKC buffer (containing 10 mM potassium phosphate, 100 mM KCl, 0.1% CHAPS) on DNA alone, DNA plus 1 μM T4-Pdg, and DNA plus 1 μM T4-Pdg plus 4 mg/ml heparin. Spectra for T4-Pdg and or heparin were collected and used for background subtraction corrections. Measurements for 2AP-containing oligonucleotides were obtained using 80 nM sample concentrations with the excitation at 315 nm (3.5 nm bandpass) and emission passed through a KV 370 filter (Schott) and into an emission monochromater scanned from 330 to 450 nm (15 nm bandpass). Measurements for TAMRA-5 were obtained using 80 nM DNA with excitation at 540 nm (1.77 nm bandpass) and emission passed through an OG 570 longpass filter (Schott) and into an emission monochromater scanned from 550 nm to 620 nm (5 nm bandpass).

Fluorescence Equilibrium Titrations

Equilibrium titrations were carried out in PKC buffer using 10, 20 or 30 nM starting oligonucleotide concentrations and adding microliter aliquots of T4-Pdg. Volume changes did not exceed 5% and titrations were corrected for dilution effects and background contributions of enzyme only controls. Mixtures were allowed to equilibrate for 1.5 min before the fluorescence intensity was recorded. Measurements for the 2-AP signal were carried out in a 1.1 ml reaction volume with excitation at 315 nm (3.5 nm bandpass) and emission was recorded at 380 nm (15 nm bandpass) using a KV-370 longpass filter. Measurements of the TAMRA signal were carried out in a 220 μl reaction volume with excitation at 550 nm (1.77 nm bandpass) and emission recorded at 585 nm (5 nm bandpass) using an OG-570 longpass filter (Schott). The Kd (app) for binding was determined from simultaneous fits of data from three DNA concentrations as described in the data analyses section.

Fluorescence Stopped-flow

Stopped-flow measurements were performed using an OLIS-USA-SF (OLIS, Jefferson, Ga.) flowbox that was attached to a SPEX fluorolog-2 fluorometer. Instrument dead-time was determined to be 3 ms. Due to either low signal intensities or small amplitude changes involved in the measurements, it was necessary to average 6–8 successive shots for each experimental determination. Data were recorded in 2 ms intervals using 2 ms signal integration. Measurements involving the 2-AP signal were performed using λ_{ex}=315 nm (3.5 nm bandpass) and λ_{em}=380 nm (15 nm bandpass) using a KV-370 emission filter (Schott). Measurements of the TAMRA signal were performed using λ_{ex}=550 nm (1.5 nm bandpass) and λ_{em}=585 nm (5 nm bandpass) using an OG-570 emission filter (Schott). Determinations of association rates were made by rapidly mixing an equal volume enzyme solution (200–700 nM) with DNA (80 nM). Determinations of dissociation rates were performed by rapidly mixing preformed ES complex (100 nM T4-Pdg, 80 nM DNA) with an equal volume of heparin (8 mg/ml).

Calculation of equilibrium binding constants

Titrations were performed by adding enzyme to fixed DNA concentrations that were near the Kd value. The data were analyzed assuming a simple binding model and data sets consisting of 10, 20 and 30 nM DNA were simultaneously fit by nonlinear regression to equation 1:

$$F_{obs}=F_o+\left(\frac{F_{\max}-F_o}{2\bullet D_t}\right)\bullet\left[(E_t+D_t+Kd)-\sqrt{(E_t+Dt+Kd)^2-(4\bullet E_t\bullet D_t)}\right] \quad (1)$$

where F_{obs} is the measured signal, F_o is the fitted initial fluorescence intensity, F_{max} is the fitted limiting fluorescence signal at saturating enzyme, E_t is the known total added enzyme concentration, D_t is the known fixed DNA concentration, and *Kd* is the fitted dissociation equilibrium constant.

Calculation of association rate constant

Stopped-flow experiments were performed under assumed pseudo first order conditions and traces were fit by nonlinear regression analysis to a single exponential rise according to equation 2:

$$F_{obs}=offset+amp\cdot(1-e^{-k_{obs}\cdot t}) \quad (2)$$

in which F_{obs} is the signal measured as a function of time, *offset* is the fitted signal at t=0, *amp* is the fitted amplitude and k_{obs} is the observed rate constant. Extracted observed rate constants were plotted against their corresponding enzyme concentrations and the bimolecular rate constant was determined from the slope of the line calculated from linear regression analysis.

Calculation of dissociation rate constants

Stopped-flow experiments were modeled as uni-molecular processes due to the irreversibility conferred by the heparin trap. Data derived from TAMRA experiments were fit to a single exponential rise according to equation 2 and 2-AP data were fit to equation 3

$$F_{obs}=offset+amp\cdot e^{-k_{obs}\cdot t} \quad (3)$$

F_{obs} is the signal measured as a function of time, *offse*t is the fitted signal at t=0, *amp* is the fitted amplitude and k_{obs} is the observed rate constant. Fits were performed by nonlinear least squares regression using KinFit (Olis, Jefferson, Ga.).

RESULTS

Characterization of the 2-AP Flipping Signal in Duplex DNA Opposite Tetrahydrofuran

Using a 21-mer duplex DNA in which a centrally located 2-AP in one strand was positioned opposite an abasic site analog, tetrahydrofuran (designated ds(2AP/TF) (Table 1), the utility of 2-AP as a nucleotide flipping signal was demonstrated by the emission spectra in the absence or presence of T4-Pdg. The excitation wavelength was set at 315 nm to isolate the 2-AP signal from any contribution from tryptophan fluorescence provided by T4-Pdg. As shown in Fig. 1, the fluorescence intensity of 2-AP in ds (2AP/TF) increased 2.8-fold when a saturating concentration of T4-Pdg was added, a result that is in excellent agreement with data previously reported (4). The enhanced signal was reversible by the addition of excess heparin, thus

demonstrating that the enhanced fluorescent signal was due to reversible binding by the enzyme. The use of heparin to compete for DNA binding enzymes has been previously described (46).

Equilibrium measurements of T4-Pdg binding to ds(2AP/TF)

The increase in intensity of 2-AP in ds(2AP/TF) upon binding by T4-Pdg provided a convenient signal to detect formation of the enzyme-DNA complex. Equilibrium experiments were performed by titrating ds(2AP/TF) with T4-Pdg and using the change in the 2-AP signal as a measure of binding. Due to the relatively weak fluorescence provided by 2-AP, it was necessary to use relatively high concentrations of the duplex DNA to acquire reliable signals. Experimental data sets consisted of three separate titrations at different DNA concentrations that were near the Kd. Global fitting of the data sets to a quadratic binding equation was performed as described in the data analysis section. Fig. 2 shows a representative data set that demonstrated that the signal increased monotonically and was saturable with increasing concentrations of T4-Pdg. Multiple data sets were analyzed with a resulting mean Kd of 28.4 ± 3.3 nM (Table 2).

Stopped-flow measurements of T4-Pdg binding

To gain further insight into the nature of the change of the 2AP signal as modulated by the addition of T4-Pdg, pre-steady state measurements were made using fluorescence stopped-flow methodology. Experiments were designed to follow the association or dissociation of the enzyme substrate complexes, using the change in the 2-AP signal as a reporter for the interaction. The association rates were measured under pseudo first order conditions by adding excess concentrations of T4-Pdg relative to ds(2AP/TF) and monitoring the increase in the 2-AP fluorescence signal. Traces from 4–9 replicate shots for each T4-Pdg concentration were averaged to improve the signal to noise ratio and were fitted to a single exponential rise to determine a pseudo first order rate constant. As shown in Fig. 3, there was a linear increase in the observed rate constants with increasing concentrations of substrate with an intrinsic association rate constant (k_{on}) of 9.78×10^8 $M^{-1}s^{-1}$ calculated by linear regression analysis.

The dissociation of the ES complex was measured by mixing preformed enzyme-DNA complexes with 8 mg/ml heparin and monitoring the decrease in the 2-AP signal (Fig. 4). Traces from 5–8 replicate shots were averaged and fitted to a single exponential decrease. These data were adequately described by a single exponential and the quality of the fits was not statistically improved upon fitting to higher order exponentials. Control experiments in which the heparin concentration was increased to 16 mg/ml did not change the results of the fits, indicating that the rate of heparin binding to free enzyme was sufficiently greater than the rebinding of enzyme to the DNA substrate (data not shown). The results were reproducible with a high degree of precision, with the average of four data sets resulting in a dissociation rate constant (k_{off}) of 24 s^{-1} (Table 2). The Kd, as calculated from the ratio of k_{off}/k_{on} was 25.6 nM and is in excellent agreement with the Kd of 28.4 nM as determined from equilibrium binding studies. This convergence of the equilibrium and pre-equilibrium results are supportive of the validity of using the 2-AP signal for monitoring the enzyme substrate interaction.

Characterization of the 2-AP fluorescence

In order to concomitantly measure nucleotide flipping and DNA bending, it was necessary to modify the ds(2AP/TF) duplex substrate by adding fluorescent donor and acceptor molecules to the two strands. Thus, this new substrate (termed ds(TAM-2AP/QSY-TF)) (Table 1) was designed with (THF) pair, an internal 2-AP/tetrahydrofuran to assess nucleotide flipping, as described above and a TAMRA/QSY-7 pair to measure DNA bending (Table 1). However, prior to conducting those investigations, it was necessary to assess whether the TAMRA/QSY-7 pair had any affect on the 2-AP emission profile. Emission spectra of this new substrate,

ds(TAM-2AP/QSY-TF), were collected in the absence or presence of T4-Pdg (Fig. 5a). The 2-AP spectra of the two duplex DNAs were indistinguishable, with comparable 2.8-fold increases in intensities in the presence of saturating T4-Pdg. This enhancement was fully reversible by the addition of heparin. These data indicate that the addition of TAMRA and QSY-7 dyes did not interfere with the flipping of the 2-AP.

Characterization of the TAMRA fluorescence

The TAMRA and QSY-7 dyes have spectral overlap and form a donor-receptor energy transfer pair. The ds(TAM-2AP/QSY-TF) substrate was designed with this pair on opposite ends of a duplex oligonucleotide, such that any change in the distance of the ends would result in a change in TAMRA intensity. Since previous structural studies had shown that T4-Pdg binding resulted in a ~60–66° kink in the DNA (5,11), experiments were carried out on this duplex to investigate whether DNA bending could be detected spectroscopically using the TAMRA/QSY-7 energy transfer pair. The emission spectrum of the TAMRA-derived signal of the duplex DNA is shown in (Fig. 5b). A 15% decrease in fluorescence intensity was observed when T4-Pdg was added. It was interpreted that this fluorescence decrease was due to the decreased distance between the dyes as a result of the bent DNA complex. The change in signal was due to reversible binding by T4-Pdg as evidenced by the fluorescent signal being restored to the original level using a heparin trap methodology. Importantly, the fluorescence change was dependent upon the presence of acceptor QSY-7. This is clearly demonstrated and shown in Fig. 5c, in which there was no effect on TAMRA fluorescence in the singly labeled duplex substrate DNA, in which the complementary strand was not labeled with QSY-7. These results are consistent with fluorescence quenching arising from the increased efficiency of energy transfer arising from the closer proximity of the ends of the DNA as a consequence of a bend caused by T4-Pdg binding.

Equilibrium measurements of T4-Pdg binding to ds(TAM-2AP/QSY-TF)

To further characterize ds(TAM-2AP/QSY-TF), equilibrium binding experiments were performed by titrating the substrate with T4-Pdg and measuring either the 2-AP or the TAMRA/QSY-7 derived signals. Titrations were performed at three concentrations of the duplex DNA and analyzed as described in the Experimental Procedures. Representative data sets are shown in Fig. 6a and 6b and the results are summarized in Table 2. The Kds obtained by measuring either 2-AP or TAMRA signals were 21.4 ± 4.2 nM and 26.7 ± 6.3 nM, respectively. The statistical equivalence of these two measurements suggests that the two signals may be reporting on the same end point (i.e. the ES complex that is both flipped and bent).

Stopped-flow Analyses

Although the equilibrium measurements using the 2-AP or TAMRA signal appear to be equivalent, a pre-steady state kinetic study was undertaken to explore for possible differences in the time-dependent changes in either signal. Stopped-flow experiments were performed by mixing a solution of preformed T4-Pdg/ds (TAM-2AP/QSY-TF) complexes with heparin and monitoring either the signal derived from 2-AP (flipping) or the TAMRA (bending) fluorescence. Due to the relatively small changes in amplitude in the TAMRA signal and fast rates encountered, it was not possible to obtain reliable association rates. Also, due to the low signal to noise ratios, between six and nine consecutive shots were averaged prior to fitting analyses. Experiments measuring the 2-AP signal in this duplex (Fig. 7a) were fit to a single exponential decrease, with a calculated average rate constant of 25 ± 1 s^{-1} (Table 2). These results were statistically indistinguishable from that obtained with ds(2AP/TF), indicating that the double-end labeling did not fundamentally alter the substrate from a mechanistic viewpoint. Interestingly, stopped-flow experiments that monitored the TAMRA/QSY-7 signal under conditions that were identical to the 2-AP measurements, resulted in dissociation rates that

were significantly faster (Fig. 7b). The traces from the TAMRA/QSY-7 data sets were adequately described by a single exponential rise and were not improved upon by fitting to higher order exponential processes. Analyses of these data resulted in an average dissociation rate constant of $62 \pm 5\ s^{-1}$ (Table 2). Additionally, there was no discernable lag corresponding to the time constant for the nucleotide flipping process.

DISCUSSION

The binding of T4-Pdg to a *cis-syn* cyclobutane pyrimidine dimer-containing DNA substrate is characterized by the formation of an ES complex in which the adenine opposite the 5′ T of the lesion is moved to an extrahelical position into a binding pocket on the enzyme with a 60°–66° kink introduced in the DNA backbone at the site of the lesion. These flipped and bent structures were evident in both cocrystal structures that have been solved for T4-pdg (5,11) and provide valuable information and insight into the mechanism of T4-Pdg. However, these structures provide only static pictures of the mechanistic processes. In order to provide a dynamic picture of the pre-catalytic events, we used oligonucleotide substrates containing strategically positioned fluorescent reporter groups. The placement of 2-AP opposite the binding site allowed measurements of nucleotide flipping, while end labeling with a donor-quencher pair allowed measurements of DNA bending. The use of the abasic site analogs as models for pyrimidine dimers is well justified since comparative analyses of the two cocrystal structures revealed only modest changes in the positioning of the extrahelical nucleotide, with most differences being in the position of specific side chains associated with the stabilization of the flipped nucleotide. Pre-steady state and equilibrium analyses of T4-Pdg interactions with these substrates provide evidence that nucleotide flipping and DNA bending occur on different time scales. This conclusion is reached from the analysis of the dissociation rates of the saturated enzyme-DNA complex in which reversal of the DNA bending signal was 2.5-fold greater in magnitude than that observed for relaxation of base flipping. The implications of these results are that base flipping and DNA bending are temporally separated on the pathway leading to the formation of the Michaelis complex. The possibility that the two events are random or can occur independent of one another is unlikely. In order to not violate the law of microscopic reversibility, two separate enzyme substrate-binding modes would need to be invoked. However, the near equivalence of the Kds measured for flipping and bending suggest similar binding interactions, presumably from the same binary complex. These conclusions are further supported based on the close similarity in the structures of the non-covalent and covalent crystal structures. Based on the correlation of the fluorescent data with the structural data, the interpretation of the enhanced fluorescence as a measure of base flipping is well justified. However, it should be noted that in the absence of analyses such as time resolved fluorescence (47), we cannot rule out definitively the possibility of other non-base-flipping distortions giving rise to the enhanced fluorescence.

Additionally, the footprint of T4-Pdg is estimated to be 11 bases, which argues against multiple enzyme molecules binding to the same oligonucleotide substrate (48). Therefore, the flipping and bending signals are measuring different intermediates in dissociation of a common complex and the 2.5-fold difference in off rates for flipping and bending indicates that flipping and bending are not simultaneous events.

The apparent association rate constant derived from the concentration-dependent linear increase in the observed k_{on} measured from 2-AP fluorescence was near the diffusion limit at $9.8 \times 10^8\ M^{-1}s^{-1}$. Using equilibrium and presteady state measurements monitoring 2-AP fluorescence, an estimate of the association rate constant, calculated as k_{off}/Kd, was $8 \times 10^8\ M^{-1}s^{-1}$. The convergence of these results is consistent with an equilibrium between the free enzyme and substrate and the flipped nucleotide complex, suggesting that the base flipping measurement is also indicative of the enzyme-DNA binding event. Additionally, in the course

of identifying substrates that would be appropriate for this study, an oligonucleotide was prepared in which the 5′ end was labeled with the fluorophore Alexa 488. The fluorescence intensity of this substrate was significantly quenched in the presence of T4-Pdg (data not shown). Stopped flow measurements of the rate of quenching of this substrate by T4-Pdg resulted in an estimation of an apparent association rate constant of approximately 9×10^8 $M^{-1}s^{-1}$. The comparable magnitude of this measurement with that of the 2-AP substrate may suggest that the enzyme-DNA interaction is near the diffusion limit and thus, nucleotide flipping is either concomitant with DNA binding or occurs in a fast step following the initial encounter. These data are similar to the results obtained for the *M. EcoRI* DNA methyltransferase, where the processes of DNA binding and base flipping were observed to be nearly simultaneous (32).

The association rate following the bending signal could not be directly measured due to signal noise relative to amplitude changes. However, an apparent association rate constant, calculated as ratio of k_{off}/Kd was approximately 2.5×10^9 $M^{-1}s^{-1}$, which is significantly greater than that determined from the flipping data or quenching experiments. Therefore, the sequential ordering of the two processes in light of these considerations leads to our proposal of a reaction pathway for T4-Pdg in which nucleotide flipping precedes DNA bending. In this interpretation, the binding of the enzyme to DNA results in the extrahelical movement of the base opposite the lesion into the binding cleft on the enzyme. This encounter is followed by a putative conformational change in which the DNA is bent. Presumably this is the structure necessary for the formation of a Michaelis complex.

Comparisons of this proposal with data derived from the analyses of other enzymes that carry out nucleotide flipping mechanisms reveal diversity in the sequential order of DNA bending and flipping. In the case of UDG, the Stivers group has demonstrated that among the earliest stages of the flipping reaction, UDG stabilizes an open state of the duplex without increasing the rate constant for spontaneous base pair opening (49). They conclude that examination of an extrahelical T of an A-T base pair occurs through a process in which the prebound enzyme transiently traps the extrahelical base without inducing a DNA bend. Concomitant studies from the Stivers group revealed that subsequent enzyme-induced DNA bending promotes the forward steps toward a fully flipped state as evidenced by loss of base-stacking interactions and the removal of hydrogen bonding (50,51). Data presented in the current study do not reveal evidence for or against a similar partial flipping model for T4-Pdg. It is also possible that there is an initial partial bend that is not kinetically observable due to exceptionally fast rates.

In contrast to these UDG data, the Verdine group presented evidence that OGG1 binds and bends non-specific and lesion-specific containing DNAs to similar extents (16). They have also demonstrated by cocrystallization of OGG1 and normal DNA that OGG1 samples normal G nucleobases in an extrahelical position that was intermediate to insertion into the enzyme active site (17). More recently, the Verdine group has demonstrated that in the process of searching for DNA lesions, MutM inserts the side chain of Phe114 into duplex DNA, buckling base pairs that remain intrahelical, while severely bending the DNA (52).

The kinetics of DNA binding, bending and nucleotide flipping have also been measured for DNA methyltransferases. Hopkins and Reich (42) used FRET analyses to determine that despite the observed bending of the cognate sequence, the binding of the *E. coli* adenine methyltransferase (*M. EcoRI*) to substrate DNA resulted in a decreased energy transfer between several combinations of donor acceptor pairs. This was explained as an expansion of the helix due to intercalation by the enzyme. The rates of DNA binding, base flipping and DNA bending for the *M. EcoRI* have been shown to be simultaneous events (42).

Collectively, these studies reveal a two- or three-step (depending on the enzyme) recognition process (specific binding, flipping, and bending) that allows several levels of regulation to help ensure proper substrate recognition before a catalytically competent ES complex is formed. Parameters that would interfere with either DNA bending or nucleotide flipping would result in an abortive encounter allowing for higher specificity.

Acknowledgements

We thank Ritche Jabil for technical assistance and Dr. M. L. Dodson for insightful discussions. This research was funded by NIH Grants ES04091 and ES06676.

References

1. Sancar A, Lindsey-Boltz LA, Unsal-Kacmaz K, Linn S. Molecular mechanisms of mammalian DNA repair and the DNA damage checkpoints. Annu Rev Biochem 2004;73:39–85. [PubMed: 15189136]
2. Huffman JL, Sundheim O, Tainer JA. DNA base damage recognition and removal: new twists and grooves. Mutat Res 2005;577:55–76. [PubMed: 15941573]
3. Lloyd RS. Investigations of pyrimidine dimer glycosylases--a paradigm for DNA base excision repair enzymology. Mutat Res 2005;577:77–91. [PubMed: 15923014]
4. McCullough AK, Dodson ML, Scharer OD, Lloyd RS. The role of base flipping in damage recognition and catalysis by T4 endonuclease V. J Biol Chem 1997;272:27210–7. [PubMed: 9341165]
5. Vassylyev DG, Kashiwagi T, Mikami Y, Ariyoshi M, Iwai S, Ohtsuka E, Morikawa K. Atomic model of a pyrimidine dimer excision repair enzyme complexed with a DNA substrate: structural basis for damaged DNA recognition. Cell 1995;83:773–82. [PubMed: 8521494]
6. Schrock, RDd; Lloyd, RS. Reductive methylation of the amino terminus of endonuclease V eradicates catalytic activities. Evidence for an essential role of the amino terminus in the chemical mechanisms of catalysis. J Biol Chem 1991;266:17631–9. [PubMed: 1894643]
7. Schrock, RDd; Lloyd, RS. Site-directed mutagenesis of the NH2 terminus of T4 endonuclease V. The position of the alpha NH2 moiety affects catalytic activity. J Biol Chem 1993;268:880–6. [PubMed: 8419366]
8. Manuel RC, Latham KA, Dodson ML, Lloyd RS. Involvement of glutamic acid 23 in the catalytic mechanism of T4 endonuclease V. J Biol Chem 1995;270:2652–61. [PubMed: 7852333]
9. Dodson ML, Schrock RDd, Lloyd RS. Evidence for an imino intermediate in the T4 endonuclease V reaction. Biochemistry 1993;32:8284–90. [PubMed: 8347626]
10. Doi T, Recktenwald A, Karaki Y, Kikuchi M, Morikawa K, Ikehara M, Inaoka T, Hori N, Ohtsuka E. Role of the basic amino acid cluster and Glu-23 in pyrimidine dimer glycosylase activity of T4 endonuclease V. Proc Natl Acad Sci U S A 1992;89:9420–4. [PubMed: 1409651]
11. Golan G, Zharkov DO, Grollman AP, Dodson ML, McCullough AK, Lloyd RS, Shoham G. Structure of T4 Pyrimidine Dimer Glycosylase in a Reduced Imine Covalent Complex with Abasic Site-containing DNA. J Mol Biol 2006;362:241–58. [PubMed: 16916523]
12. Slupphaug G, Mol CD, Kavli B, Arvai AS, Krokan HE, Tainer JA. A nucleotide-flipping mechanism from the structure of human uracil-DNA glycosylase bound to DNA [see comments]. Nature 1996;384:87–92. [PubMed: 8900285]
13. Barrett TE, Savva R, Panayotou G, Barlow T, Brown T, Jiricny J, Pearl LH. Crystal structure of a G:T/U mismatch-specific DNA glycosylase: mismatch recognition by complementary-strand interactions. Cell 1998;92:117–29. [PubMed: 9489705]
14. Lau AY, Scharer OD, Samson L, Verdine GL, Ellenberger T. Crystal structure of a human alkylbase-DNA repair enzyme complexed to DNA: mechanisms for nucleotide flipping and base excision. Cell 1998;95:249–58. [PubMed: 9790531]
15. Hollis T, Lau A, Ellenberger T. Structural studies of human alkyladenine glycosylase and E. coli 3-methyladenine glycosylase. Mutat Res 2000;460:201–10. [PubMed: 10946229]
16. Chen L, Haushalter KA, Lieber CM, Verdine GL. Direct visualization of a DNA glycosylase searching for damage. Chem Biol 2002;9:345–50. [PubMed: 11927259]

17. Banerjee A, Yang W, Karplus M, Verdine GL. Structure of a repair enzyme interrogating undamaged DNA elucidates recognition of damaged DNA. Nature 2005;434:612–8. [PubMed: 15800616]
18. Fromme JC, Verdine GL. Structural insights into lesion recognition and repair by the bacterial 8-oxoguanine DNA glycosylase MutM. Nat Struct Biol 2002;9:544–52. [PubMed: 12055620]
19. Gilboa R, Zharkov DO, Golan G, Fernandes AS, Gerchman SE, Matz E, Kycia JH, Grollman AP, Shoham G. Structure of formamidopyrimidine-DNA glycosylase covalently complexed to DNA. J Biol Chem 2002;277:19811–6. [PubMed: 11912217]
20. Serre L, Pereira de Jesus K, Boiteux S, Zelwer C, Castaing B. Crystal structure of the Lactococcus lactis formamidopyrimidine-DNA glycosylase bound to an abasic site analogue-containing DNA. Embo J 2002;21:2854–65. [PubMed: 12065399]
21. Doublie S, Bandaru V, Bond JP, Wallace SS. The crystal structure of human endonuclease VIII-like 1 (NEIL1) reveals a zincless finger motif required for glycosylase activity. Proc Natl Acad Sci U S A 2004;101:10284–9. [PubMed: 15232006]
22. Zharkov DO, Golan G, Gilboa R, Fernandes AS, Gerchman SE, Kycia JH, Rieger RA, Grollman AP, Shoham G. Structural analysis of an Escherichia coli endonuclease VIII covalent reaction intermediate. Embo J 2002;21:789–800. [PubMed: 11847126]
23. Daujotyte D, Serva S, Vilkaitis G, Merkiene E, Venclovas C, Klimasauskas S. HhaI DNA methyltransferase uses the protruding Gln237 for active flipping of its target cytosine. Structure (Camb) 2004;12:1047–55. [PubMed: 15274924]
24. Jiang YL, Kwon K, Stivers JT. Turning On uracil-DNA glycosylase using a pyrene nucleotide switch. J Biol Chem 2001;276:42347–54. [PubMed: 11551943]
25. Handa P, Roy S, Varshney U. The role of leucine 191 of Escherichia coli uracil DNA glycosylase in the formation of a highly stable complex with the substrate mimic, ugi, and in uracil excision from the synthetic substrates. J Biol Chem 2001;276:17324–31. [PubMed: 11278852]
26. Parikh SS, Mol CD, Slupphaug G, Bharati S, Krokan HE, Tainer JA. Base excision repair initiation revealed by crystal structures and binding kinetics of human uracil-DNA glycosylase with DNA. EMBO J 1998;17in press
27. Parikh SS, Walcher G, Jones GD, Slupphaug G, Krokan HE, Blackburn GM, Tainer JA. Uracil-DNA glycosylase-DNA substrate and product structures: conformational strain promotes catalytic efficiency by coupled stereoelectronic effects. Proc Natl Acad Sci U S A 2000;97:5083–8. [PubMed: 10805771]
28. Guan Y, Manuel RC, Arvai AS, Parikh SS, Mol CD, Miller JH, Lloyd S, Tainer JA. MutY catalytic core, mutant and bound adenine structures define specificity for DNA repair enzyme superfamily. Nat Struct Biol 1998;5:1058–64. [PubMed: 9846876]
29. Scharer OD, Ortholand JY, Ganesan A, Ezaz-Nikpay K, Verdine GL. Specific binding of the DNA repair enzyme AlkA to a pyrrolidine-based inhibitor. J Am Chem Soc 1995;117:6623–24.
30. Scharer OD, Kawate T, Gallinari P, Jiricny J, Verdine GL. Investigation of the mechanisms of DNA binding of the human G/T glycosylase using designed inhibitors. Proc Natl Acad Sci U S A 1997;94:4878–83. [PubMed: 9144158]
31. McCullough AK, Scharer O, Verdine GL, Lloyd RS. Structural determinants for specific recognition by T4 endonuclease V. J Biol Chem 1996;271:32147–52. [PubMed: 8943268]
32. Allan BW, Reich NO, Beechem JM. Measurement of the absolute temporal coupling between DNA binding and base flipping. Biochemistry 1999;38:5308–14. [PubMed: 10220317]
33. Gowher H, Jeltsch A. Molecular enzymology of the EcoRV DNA-(Adenine-N (6))-methyltransferase: kinetics of DNA binding and bending, kinetic mechanism and linear diffusion of the enzyme on DNA. J Mol Biol 2000;303:93–110. [PubMed: 11021972]
34. Reddy YV, Rao DN. Binding of EcoP15I DNA methyltransferase to DNA reveals a large structural distortion within the recognition sequence. J Mol Biol 2000;298:597–610. [PubMed: 10788323]
35. Wong I, Lundquist AJ, Bernards AS, Mosbaugh DW. Presteady-state analysis of a single catalytic turnover by Escherichia coli uracil-DNA glycosylase reveals a “pinch-pull-push” mechanism. J Biol Chem 2002;277:19424–32. [PubMed: 11907039]
36. Stivers JT, Pankiewicz KW, Watanabe KA. Kinetic mechanism of damage site recognition and uracil flipping by Escherichia coli uracil DNA glycosylase. Biochemistry 1999;38:952–63. [PubMed: 9893991]

37. Jiang YL, Stivers JT. Mutational analysis of the base-flipping mechanism of uracil DNA glycosylase. Biochemistry 2002;41:11236–47. [PubMed: 12220189]
38. Zhao X, Liu J, Hsu DS, Zhao S, Taylor JS, Sancar A. Reaction mechanism of (6–4) photolyase. J Biol Chem 1997;272:32580–90. [PubMed: 9405473]
39. Vande Berg BJ, Sancar GB. Evidence for dinucleotide flipping by DNA photolyase. J Biol Chem 1998;273:20276–84. [PubMed: 9685377]
40. Christine KS, MacFarlane AWt, Yang K, Stanley RJ. Cyclobutylpyrimidine dimer base flipping by DNA photolyase. J Biol Chem 2002;277:38339–44. [PubMed: 12169694]
41. Allan BW, Garcia R, Maegley K, Mort J, Wong D, Lindstrom W, Beechem JM, Reich NO. DNA bending by EcoRI DNA methyltransferase accelerates base flipping but compromises specificity. J Biol Chem 1999;274:19269–75. [PubMed: 10383435]
42. Hopkins BB, Reich NO. Simultaneous DNA binding, bending, and base flipping: evidence for a novel M. EcoRI methyltransferase-DNA complex. J Biol Chem 2004;279:37049–60. [PubMed: 15210696]
43. Huang N, Banavali NK, MacKerell AD Jr. Protein-facilitated base flipping in DNA by cytosine-5-methyltransferase. Proc Natl Acad Sci U S A 2003;100:68–73. [PubMed: 12506195]
44. Jaruga P, Jabil R, McCullough AK, Rodriguez H, Dizdaroglu M, Lloyd RS. Chlorella virus pyrimidine dimer glycosylase excises ultraviolet radiation- and hydroxyl radical-induced products 4,6-diamino-5-formamidopyrimidine and 2,6-diamino-4-hydroxy-5-formamidopyrimidine from DNA. Photochem Photobiol 2002;75:85–91. [PubMed: 11883607]
45. Pace CN, Vajdos F, Fee L, Grimsley G, Gray T. How to measure and predict the molar absorption coefficient of a protein. Protein Sci 1995;4:2411–23. [PubMed: 8563639]
46. Iakoucheva LM, Walker RK, van Houten B, Ackerman EJ. Equilibrium and stop-flow kinetic studies of fluorescently labeled DNA substrates with DNA repair proteins XPA and replication protein A. Biochemistry 2002;41:131–43. [PubMed: 11772010]
47. Neely RK, Daujotyte D, Grazulis S, Magennis SW, Dryden DT, Klimasauskas S, Jones AC. Time-resolved fluorescence of 2-aminopurine as a probe of base flipping in M. HhaI-DNA complexes. Nucleic Acids Res 2005;33:6953–60. [PubMed: 16340006]
48. Latham KA, Manuel RC, Lloyd RS. The interaction of T4 endonuclease V E23Q mutant with thymine dimer- and tetrahydrofuran-containing DNA. J Bacteriol 1995;177:5166–8. [PubMed: 7665500]
49. Cao C, Jiang YL, Stivers JT, Song F. Dynamic opening of DNA during the enzymatic search for a damaged base. Nat Struct Mol Biol 2004;11:1230–6. [PubMed: 15558051]
50. Krosky DJ, Schwarz FP, Stivers JT. Linear free energy correlations for enzymatic base flipping: how do damaged base pairs facilitate specific recognition? Biochemistry 2004;43:4188–95. [PubMed: 15065862]
51. Krosky DJ, Song F, Stivers JT. The origins of high-affinity enzyme binding to an extrahelical DNA base. Biochemistry 2005;44:5949–59. [PubMed: 15835884]
52. Banerjee A, Santos WL, Verdine GL. Structure of a DNA glycosylase searching for lesions. Science 2006;311:1153–7. [PubMed: 16497933]

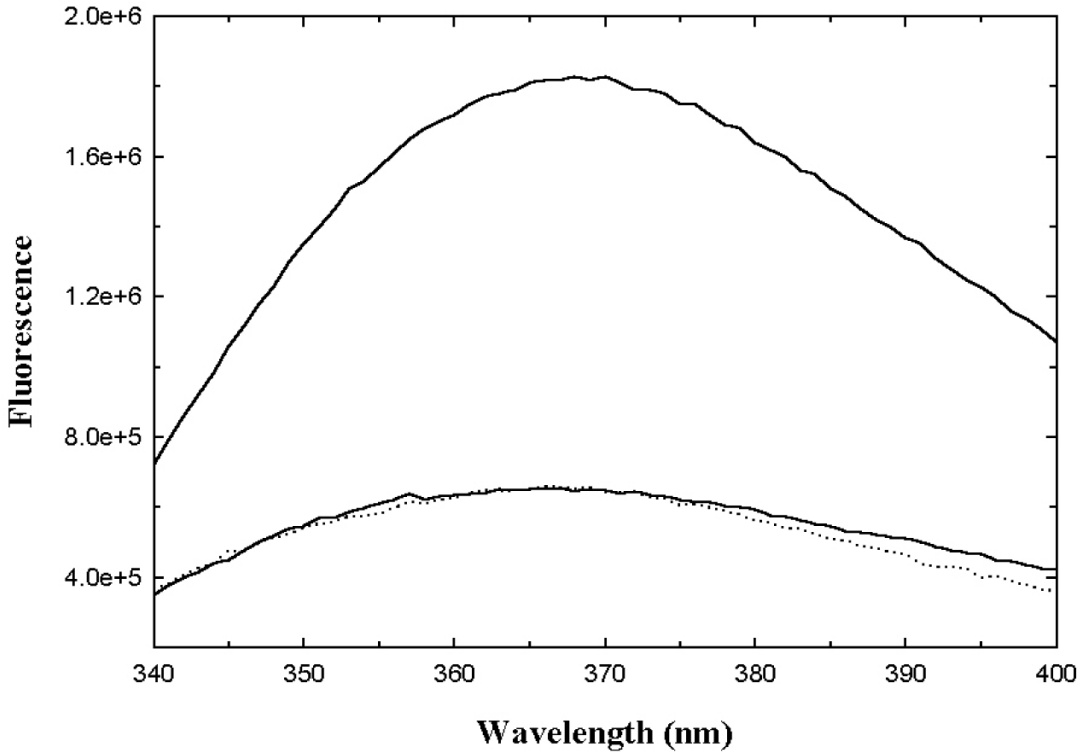

Figure 1. Fluorescence spectra for ds(2AP/TF) in the presence or absence of T4-Pdg

Measurements were made in 10 mM KH_2PO_4, 100 mM KCl, 0.1% CHAPS, pH 6.8 at 25° C. Samples were 80 nM ds(2AP/TF) (lower solid line), 80 nM ds(2AP/TF) plus 1 μM T4-Pdg (upper solid line) or ds(2AP/TF) plus 1 μM T4-Pdg and 4 mg/ml heparin (dotted line). Spectra were recorded using λ_{ex}=315 nm and λ_{em}=380 nm.

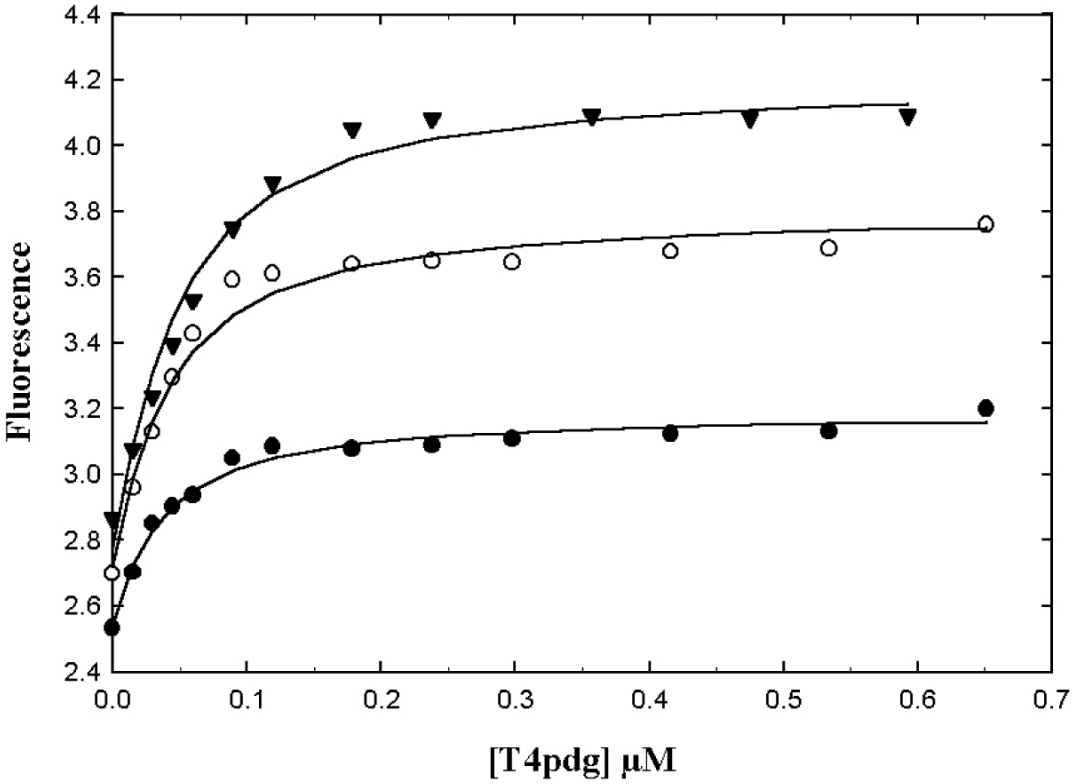

Figure 2. Equilibrium binding measurements of T4-Pdg and ds(2AP/TF)

Titrations were performed in PKC buffer using three fixed concentrations of ds(2AP/TF) corresponding to 10 nM (●), 20 nM (O), and 30 nM (θ). The lines drawn are from a global fit of the data described in the data analysis section. Shown is a representative data set with Kd = 24.9 ± 10.2 nM.

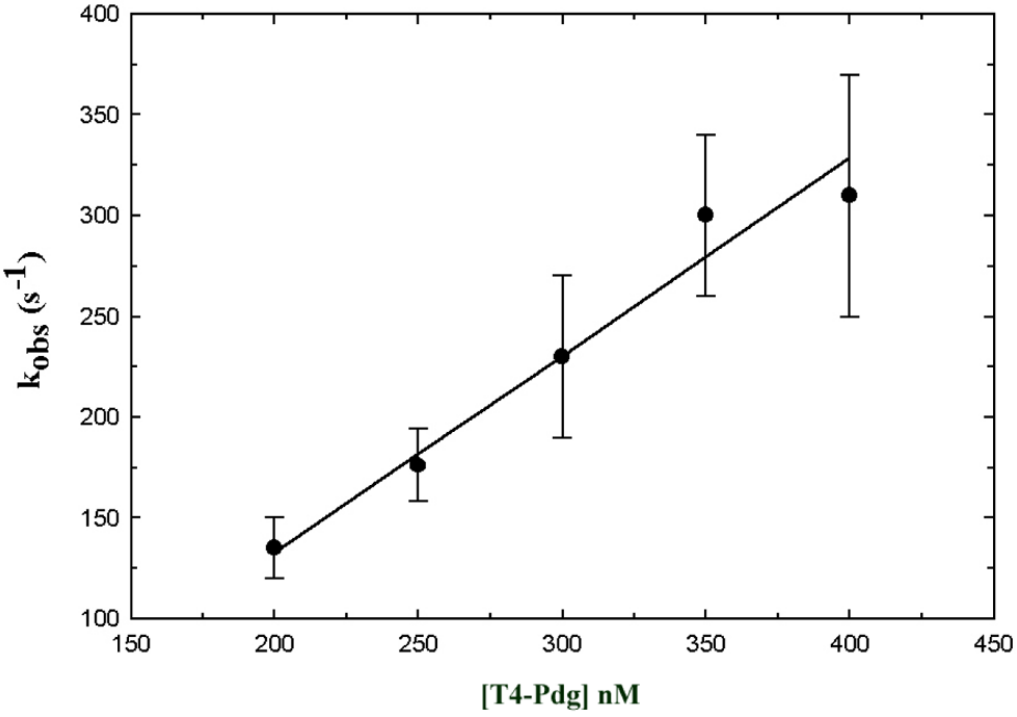

Figure 3. Association rate constant for T4-Pdg and ds(2AP/TF)

Pseudo-first order rate constants for the association of ds(2AP/TF) with T4-Pdg were determined by fluorescence stopped-flow experiments in PKC buffer using 80 nM ds(2AP/TF) (syringe A) and increasing concentrations of T4-Pdg (syringe B). The values determined were derived from between four to nine replicate traces and are plotted with error bars corresponding to the 95% confidence limits. The line drawn is from weighted linear regression analysis using the relative errors in the k_{obs} values to obtain an intrinsic association rate constant of $9.78 \times 10^8 \pm 0.2\ M^{-1}s^{-1}$.

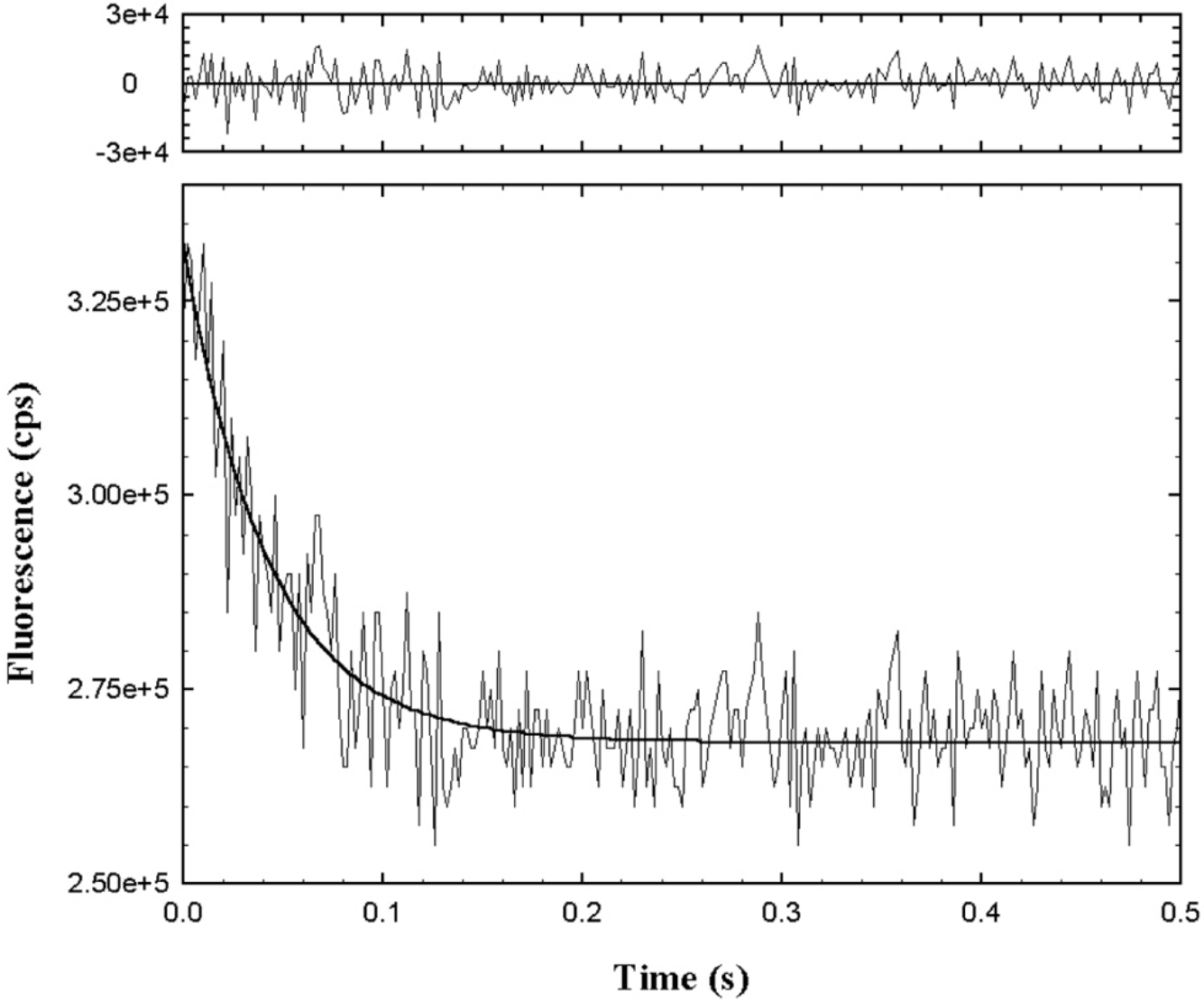

Figure 4. Dissociation rate constant for T4-Pdg and ds(2AP/TF)

Dissociation rate constants were determined by fluorescence stopped-flow measurements. Experiments were performed in PKC buffer by mixing 80 nM plus 200 nM T4-Pdg (syringe A) with 8 mg/ml heparin (syringe B). Data were recorded in 2 ms steps with excitation λ_{ex}=315 nm and λ_{em} = 380. Between 5–8 traces were averaged and fit to a single exponential as described in the data analysis section. Shown is a representative data set with k_{off} = 23.6 ± 1.4 s^{-1}. The residuals to the fitted line are shown in the upper panel.

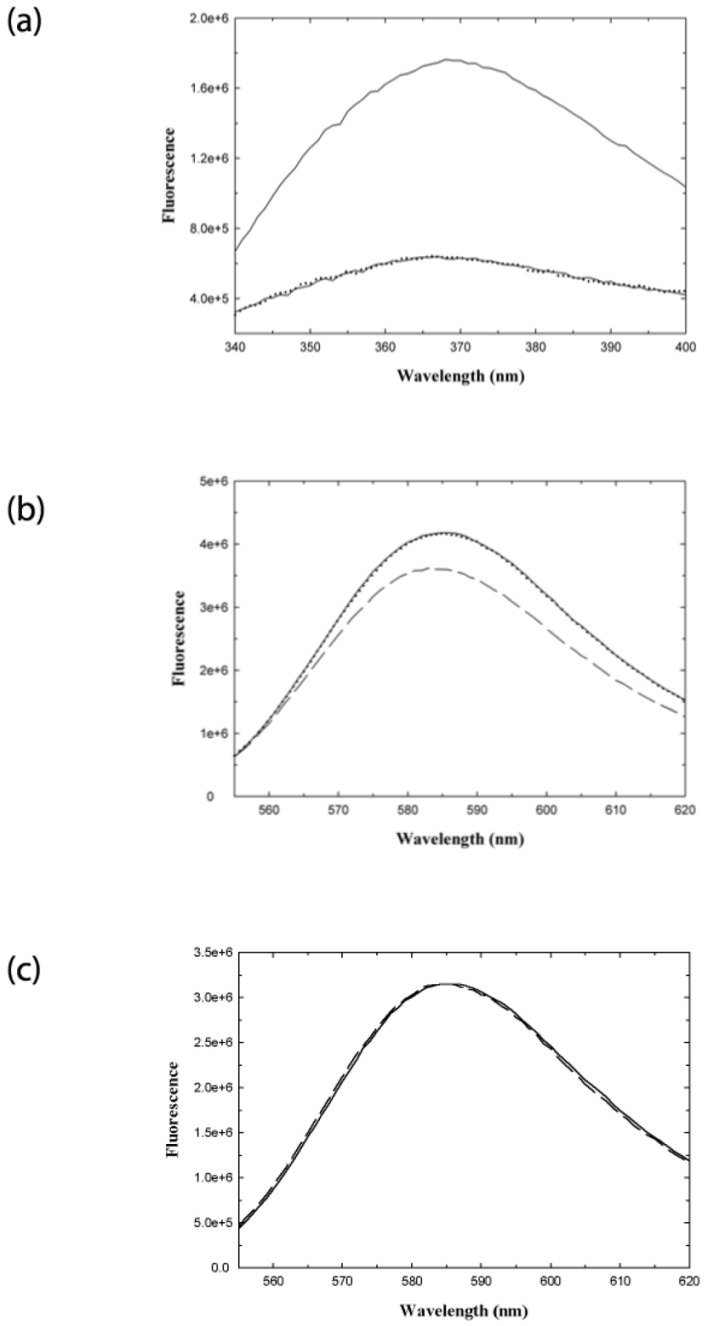

Figure 5. Fluorescence spectra of ds(TAM-2AP/QSY-TF) and ds(TAM-2AP/TF) in the presence or absence of T4-Pdg

Measurements were made in PKC buffer at 25° C. *(a)* 2-AP fluorescence samples were 80 nM ds(TAM-2AP/QSY-TF) (solid lower line), 80 nM ds(TAM-2AP/QSY-TF) plus 1 μM T4-Pdg (solid upper line) or ds(TAM-2AP/QSY-TF) plus 1 μM T4-Pdg and 4 mg/ml heparin (dotted line). Spectra were recorded using λ_{ex}=315 nm and λ_{em}=380 nm. *(b)* TAMRA fluorescence samples were 80 nM ds(TAM-2AP/QSY-TF) (solid line), 80 nM ds(TAM-2AP/QSY-TF) plus 1 μM T4-Pdg (dashed line) or ds(TAM-2AP/QSY-TF) plus 1 μM T4-Pdg and 4 mg/ml heparin (dotted line). Spectra were recorded using λ_{ex}=550 nm and λ_{em}=585 nm. *(c)* TAMRA fluorescence dependent on QSY-7 samples were 80 nM ds(TAM-2AP/TF) (solid line), 80 nM

ds(TAM-2AP/TF) plus 1 μM T4-Pdg (dashed line). Spectra were recorded using λ_{ex}=550 nm and λ_{em}=585 nm.

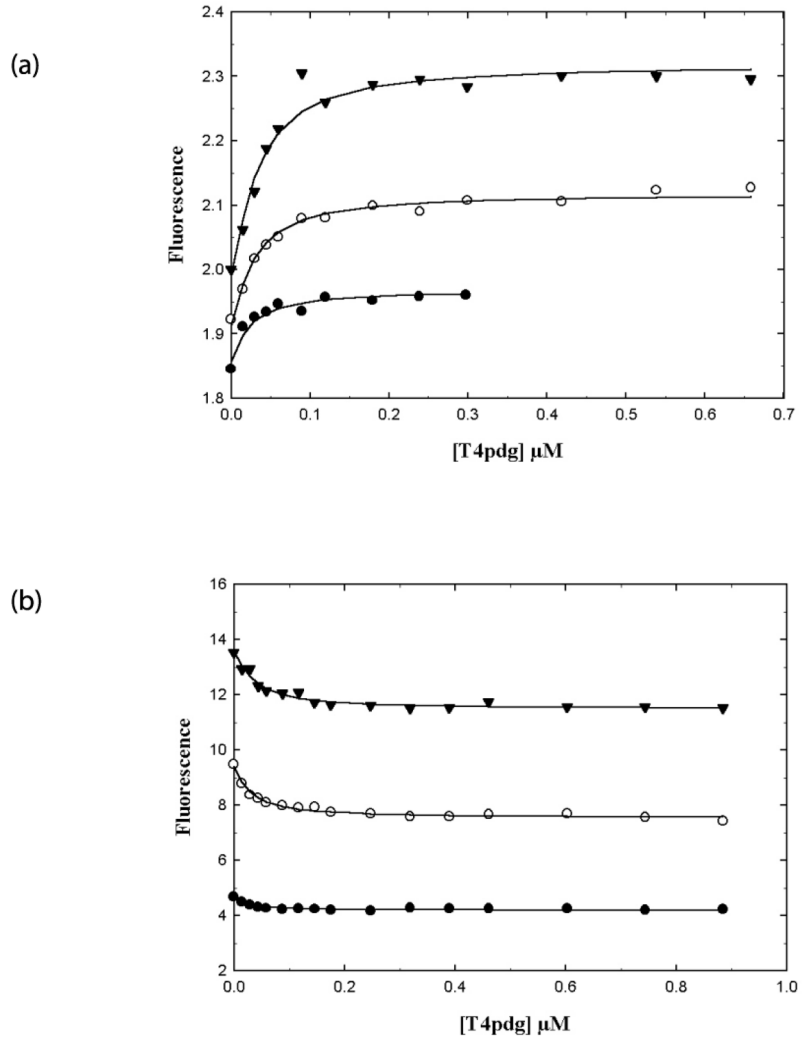

Figure 6. Equilibrium binding measurements of T4-Pdg with ds(TAM-2AP/QSY-TF)

Titrations were performed in PKC buffer at three fixed concentrations of ds(TAM-2AP/QSY-TF) at 10 nM (●), 20 nM (O), and 30 nM (θ). The lines drawn are from a global fit of the data as described in the data analysis section. *(a)* 2-AP Fluorescence shown is a representative data set using λ_{ex} = 315 nm and λ_{em} = 380 nm with Kd = 19 ± 6.1 nM. *(b)* TAMRA fluorescence shown is a representative data set using λ_{ex} = 550 nm and λ_{em} = 585 nm with Kd = 21.43 ± 5.3 nM.

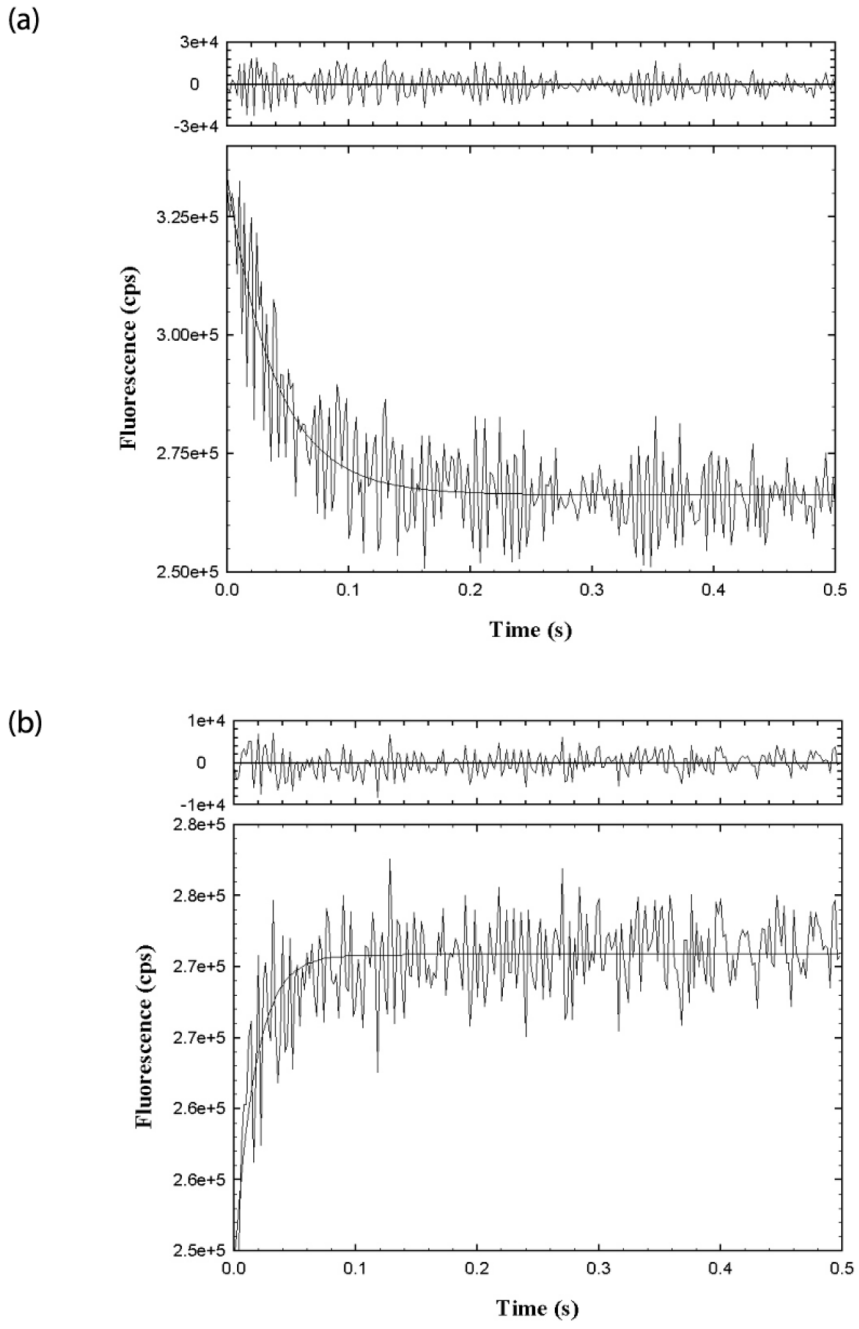

Figure 7. Dissociation of the ds(TAM-2AP/QSY-TF)/T4-Pdg complex following the 2-AP nucleotide flipping signal and the TAMRA DNA bending signal

Dissociation rate constants were determined by fluorescence stopped-flow measurements. Experiments were performed in PKC buffer by mixing 80 nM plus 200 nM T4-Pdg (syringe A) with 8 mg/ml heparin (syringe B). *(a)* 2-AP nucleotide flipping signal: data were recorded in 2 ms steps with excitation λ_{ex}=315 nm and λ_{em} = 380. Between 6–9 traces were averaged and fit to a single exponential fall as described in the data analysis section. Shown is a representative data set with $k_{off} = 24.1 \pm 1.2 s^{-1}$. The residuals to the fitted line are shown in the upper panel. *(b)* TAMRA DNA bending signal: data were recorded in 2 ms steps with excitation λ_{ex}=550 nm and λ_{em} = 585. Between 6–9 traces were averaged and fit to a single

exponential rise as described in the data analysis section. Shown is a representative data set with $k_{off} = 59 \pm 7\ s^{-1}$. The residuals to the fitted line are shown in the upper panel.

Table 1

Duplex oligonucleotide substrates.[a]

ds(2AP/TF)	GTTCCAGCTA2GCTCAGGTTC CAAGGTCGATdCGAGTCCAAG
ds(TAM-2AP/TF)	TAM-GTTCCAGCTA2GCTCAGGTTC CAAGGTCGATdCGAGTCCAAG
ds(TAM-2AP/QSY-TF)	TAM-GTTCCAGCTA2GCTCAGGTTC CAAGGTCGATdCGAGTCCAAG-QSY

[a] 5′→3′ (top strand)

TAM: TAMRA

QSY: QSY-7

d=TF: tetrahydrofuran

2: 2-aminopurine

Table 2

Summary of kinetic and equilibrium constants derived for T4-Pdg with ds(2AP/TF) and ds(TAM-2AP/QSY-TF) substrates.

Substrate	Kd (nM) [e]	Kd (nM)[f]	k_{on} ($M^{-1}s^{-1}$)[e]	k_{off} (s^{-1})[b,e]	k_{off} (s^{-1})[b,f]
ds(2AP/TF)	28.4 ± 3.3[a]	nd	$9.78 \times 10^8 \pm 0.2$	24 ± 2.5[c]	nd
ds(TAM-2AP/QSY-TF)	21.4 ± 4.2[a]	26.7 ± 6.3[a]	nd	25 ± 1[c]	62 ± 5[d]

[a]: Mean ± SD n=3

[b]: 6–9 replicate shots were collected and averaged per stopped-flow experiment.

[c]: Mean ± SD n=4

[d]: Mean ± SD n=5

[e]: estimated from 2-AP fluorescence

[f]: estimated from FRET analyses